

Modeling of flux enhancement in presence of concentration polarization by pressure pulsation during laminar cross flow ultrafiltration

Kamal Kumar and Sirshendu De*

Department of Chemical Engineering, Indian Institute of Technology, Kharagpur, Kharagpur - 721 302, India
(Received September 11, 2009, Accepted June 16, 2010)

Abstract. A theoretical study for the flux enhancement by pulsation of transmembrane pressure is presented for osmotic pressure controlled ultrafiltration under laminar flow regime. The transient velocity profile is solved analytically using Green's function method. Time dependent convective diffusive equation is solved to quantify the membrane surface concentration and the permeate flux, numerically. The effects of the amplitude and frequency of pulsation on flux, surface concentration and observed retention are studied.

Keywords: pulsatile flow; osmotic pressure controlling; ultrafiltration; permeate flux; retention.

1. Introduction

Osmotic pressure controlled cross flow ultrafiltration has become an efficient and less energy consuming unit operation for separation, concentration and fractionation of various important process streams containing proteins, polymers, etc. However, decline in flux due to membrane fouling is the major problem in the membrane based separation processes. Membrane fouling is generally divided into reversible and irreversible fouling. In reversible fouling, solute concentration near the membrane surface becomes more or there is a formation of gel type layer over the membrane surface depending on the nature of solutes to be filtered. In this case, the deposition over the membrane surface can be removed with an appropriate cleaning protocol. In case of irreversible fouling, the solutes may be adsorbed on the pore mouth or inside the pore by blocking the pores partially or completely (Pradanos *et al.* 1996). Many techniques to reduce the flux decline have been summarized in several review articles (Ilias and Govind 1990, Spiazi *et al.* 1993, Winzeler and Belfort 1993, Wakeman and Williams 2002). Based on the specific causes for flux decline, the control strategies are mainly undertaken in the following directions, namely, (i) modification of the membranes, (ii) modification of the feed, (iii) use of external field, *e.g.*, electric, magnetic, sonic, etc., (iv) modification of the hydrodynamics in the flow channel. Modification of the membrane materials includes alteration of the membrane surface by specific treatments, such as, surfactants, plasma treatments, etc., (Pal *et al.* 2008a). It is reported that the membrane surface treated by CO₂ plasma makes the surface more hydrophilic, leading to a flux enhancement by about 15-20% (Pal *et al.* 2008b). In case of filtration of charged macromolecules, such as, proteins, pectin, etc., suitable use of external electric field

* Corresponding author, Professor, E-mail: sde@che.iitkgp.ernet.in

reduces the concentration polarization and consequently, enhances the permeate flux significantly. Application of direct current electric field is reported to enhance the permeate flux of mosambi juice upto 30% (Sarkar *et al.* 2008a, Sarkar *et al.* 2008b). For filtration of protein bovine serum albumin, electric field can enhance the permeate flux even upto 100% (Sarkar *et al.* 2008c). Modification of the hydrodynamics is the most popular approach. Modification of hydrodynamics can be achieved by simply using turbulent promoter or changing the flow regime from laminar to turbulent. Reports of use of turbulent promoters and turbulent flow regime to enhance the permeate flux is abundant in literature (Krstic *et al.* 2002, Ahmad *et al.* 2005, Das *et al.* 2007, Das *et al.* 2008). It is reported that about 20 to 50% flux enhancement is possible using turbulent promoters and turbulent flow regime for treatment of tannery effluents depending upon the operating conditions (Das *et al.* 2007, Das *et al.* 2008). Imposition of pulsatile flow in the membrane module is another technique for modifying the hydrodynamics in the flow channel.

Alteration of the module hydrodynamics by pulsation can be induced by transmembrane pressure pulsation (Rodgers and Sparks 1991, Li *et al.* 1998, Curcio *et al.* 2002) or retentate flow rate pulsation (Najrain and Bellhouse 1998, Jaffrin *et al.* 1994, Wang *et al.* 1994). Induction of flow rate pulsation by collapsible tube pulsation generator is also available in the literature for a microfiltration system (Hadzismajlovic and Bertram 1998a, Hadzismajlovic and Bertram 1998b). It is reported that the flux enhancement in the cross flow microfiltration can be as high as 450% for laminar flow (Hadzismajlovic and Bertram 1998a) and upto 120% for turbulent flow regime (Hadzismajlovic and Bertram 1998b). It is reported that the transmembrane pressure pulsation is more effective than the flow rate pulsation (Rodgers and Sparks 1992). In a recent study, it is reported that up to 300% flux enhancement is achieved by using flow pulsation during microfiltration of bentonite solution (Wang *et al.* 2007). It may be noted that most of the works carried out to investigate the effects of the pulsatile flow are restricted to cross flow microfiltration (Bertram *et al.* 1993, Gupta *et al.* 1992, Jaffrin 1989) and the works available are mostly experimental in nature. However, the effects of the pulsatile flow on the performance of the osmotic pressure controlled cross flow ultrafiltration is scant in the literature and a theoretical approach to model such system is rare.

In the present work, an attempt has been made to model the effects of transmembrane pressure pulsation during osmotic pressure controlled cross flow ultrafiltration under laminar flow regime. The nature of the pulsation of the resulting cross flow velocity is identified to effect the improvement of the permeate flux. The transient velocity profile is solved analytically using Green's function method with an assumed periodic variation of the axial pressure drop profile. The convective diffusion equation is numerically solved using the developed velocity profile to obtain the profile of the membrane surface concentration and the permeate flux. The limiting value for the selection of the amplitude and the frequency of pulsation is obtained. Finally, the maximum flux enhancement possible in such case is quantified. It may be mentioned that the experimental data of flux enhancement with pressure pulsation is available for cake/gel controlling ultrafiltration (Hadzismajlovic and Bertram 1998a, Wang *et al.* 2007) but are unavailable for osmotic pressure controlled filtration. Therefore, the present work is completely a modeling and simulation work. In case of water treatment, either drinking water by reverse osmosis or sewage water treatment by ultrafiltration, pressure pulsation can be one alternative to enhance the permeate flux. The present model can be of extremely helpful in designing and scaling up of such systems.

2. Theory

The flow geometry is shown in Fig. 1. Fluid is allowed to flow tangentially over the membrane surface. The permeate flux is a function of the channel length for the module. The concentration boundary layer develops over the effective length of the membrane. It is assumed that flow inside the channel is laminar and fully developed before imposition of the pulsation. The cross-sectional averaged velocity prevailing in the channel before pulsation is given by (Bird *et al.* 2002),

$$u_0 = \frac{h^2}{12\mu} \left(\frac{dP}{dx} \right)_0 \tag{1}$$

where, u_0 is the cross sectional average velocity, h is the half height of the channel, μ is the solution viscosity and $\left(\frac{dP}{dx} \right)_0$ is the pressure gradient. A periodic variation of the axial pressure gradient as follows is now introduced in the system,

$$\left(\frac{dP}{dx} \right) = \left(\frac{dP}{dx} \right)_0 (1 + k \cos(\omega t)) \tag{2}$$

Since, the permeate side pressure is atmospheric pressure, P in the above equation is equivalent to transmembrane pressure drop at any location x . k is the amplitude and ω is the frequency of periodic fluctuation.

2.1 Transient velocity profile

Initially, the fully developed laminar velocity profile exists in the flow channel. At $t > 0$, the pressure gradient changes periodically following Eq. (2). The transient velocity profile can be obtained using the x -component equation of motion as,

$$\rho \frac{\partial u}{\partial t} = - \frac{\partial P}{\partial x} + \mu \frac{\partial^2 u}{\partial y^2} \tag{3}$$

where, ρ is the density and u is the x -component of velocity. Inserting the profile for the pressure

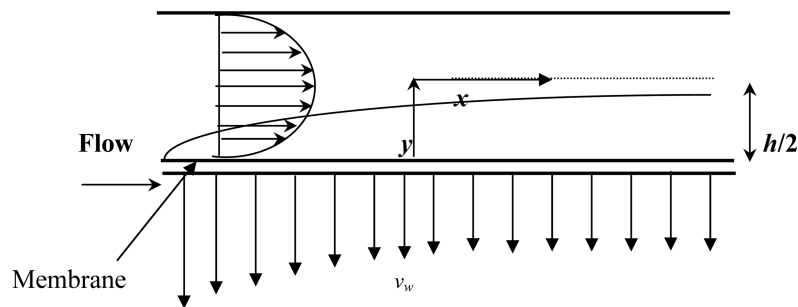


Fig. 1 Schematic of the cross flow system

gradient given by Eq. (2), the following equation results,

$$\rho \frac{\partial u}{\partial t} = \left(-\frac{dP}{dx} \right)_0 (1 + k \cos(\omega t)) + \mu \frac{\partial^2 u}{\partial y^2} \quad (4)$$

The above equation is expressed in terms of the following non-dimensional variables,

$$y^* = \frac{y}{h}, \quad t^* = \frac{t\nu}{h^2}, \quad u^* = \frac{u}{u^0} \quad (5)$$

Eq. (4) can be non-dimensionalized as,

$$\frac{\partial u^*}{\partial t^*} = \alpha [1 + k \cos(\beta t^*)] + \frac{\partial^2 u^*}{\partial y^{*2}} \quad (6)$$

where, $\alpha = \left(-\frac{dP}{dx} \right)_0 \frac{h^2}{\mu u^0}$ and $\beta = \frac{\omega h^2}{\nu}$.

The initial and boundary conditions of Eq. (6) in terms of the non-dimensional variables are,

$$\text{at } t^* = 0, \quad u^* = 6(y^* - y^{*2}) \quad (7)$$

$$\text{at } y^* = 0, \quad u^* = 0 \quad (8)$$

$$\text{at } y^* = 1, \quad u^* = 0 \quad (9)$$

Eq. (6) is solved using Green's function method and the analytical solution of the transient velocity profile is obtained as presented in the Appendix,

$$\begin{aligned} u^*(y^*, t^*) = & 24 \sum_{n=1}^{\infty} \frac{(1 - \cos(n\pi))}{n^3 \pi^3} \sin(n\pi y^*) e^{-n^2 \pi^2 t^*} \\ & + 2\alpha \sum_{n=1}^{\infty} \frac{(1 - \cos n\pi)}{n\pi} \sin(n\pi y^*) \left[\frac{1 - e^{-n^2 \pi^2 t^*}}{n^2 \pi^2} + \frac{k}{n^4 \pi^4 + \beta^2} (n^2 \pi^2 \cos \beta t^* + \beta \sin \beta t^* - n^2 \pi^2 e^{-n^2 \pi^2 t^*}) \right] \end{aligned} \quad (10)$$

The cross-sectional averaged velocity profile can be obtained as

$$u^*_{ya} = \int_0^1 u^* dy^* \quad (11)$$

In order to check the validity of the transient velocity profile developed by Eq. (10), Eq. (6) is solved numerically using a finite difference scheme. A comparison of the cross-sectional average velocity ((Eq. (11)), computed using the analytical solution ((Eq. (10)) and the numerical solution of Eq. (6) by finite difference, is presented in Fig. 2, for various values of the amplitude (k) and frequency (ω) of oscillation. The figure shows that the analytical solution by Eq. (10) is an exact one.

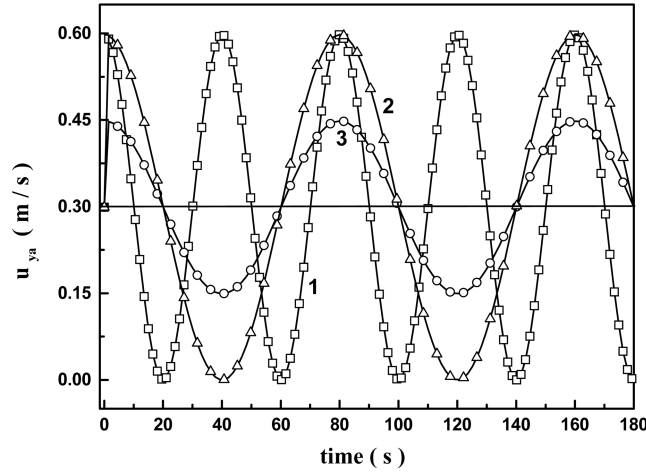


Fig. 2 Comparison of the analytical and numerical solution of the y -averaged velocity with k and ω at $\Delta P = 550$ kPa, $c_o = 10$ kg/m³ and $u_o = 0.3$ m/s. Solid line – Analytical solution; Symbols – Numerical solution (1) $k = 1.0$, $\omega = 0.157$ Hz; (2) $k = 1.0$, $\omega = 0.0785$ Hz; (3) $k = 0.5$, $\omega = 0.0785$ Hz

2.2 Profile of the transmembrane pressure drop

The pressure profile along the channel length at any time point can be obtained by integrating Eq. (2) as,

$$P = P_i - \left(\frac{dP}{dx} \right)_0 [1 + k \cos(\omega t)] x \quad (12)$$

where, P_i is the inlet pressure and $\left(\frac{dP}{dx} \right)_0$ is the inlet pressure drop. Subtracting $P_{permeate}$ on both sides of Eq. (12), the expression for the transmembrane pressure drop can be obtained as,

$$\Delta P = \Delta P_i - \left(\frac{dP}{dx} \right)_0 [1 + k \cos(\omega t)] x \quad (13)$$

2.3 Profiles of the membrane surface concentration and the permeate flux along the channel

The following assumptions are made in the development of the profiles of the membrane surface concentration and that of the permeate flux: (i) diffusion along the channel is negligible compared to convection in the same direction, (ii) permeate velocity is small enough compared to the feed velocity, keeping the velocity profile in the major part of the channel one dimensional. However, within the thin concentration boundary layer the flow is two-dimensional (as the mass transfer is taking place in the y -direction as well) (iii) physical properties of the solution are constant.

Therefore, the solute mass balance equation inside the concentration boundary layer can be written as,

$$\frac{\partial c}{\partial t} + u \frac{\partial c}{\partial x} + v \frac{\partial c}{\partial y} = D \frac{\partial^2 c}{\partial y^2} \quad (14)$$

where, c is solute concentration, v is transverse (y -component) velocity component and D is the solute diffusivity. The axial velocity profile, u , is expressed by Eq. (10). The transverse velocity profile may be expressed as (Bouchard *et al.* 1994),

$$v = -v_w \quad (15)$$

where, v_w is the osmotic pressure controlled permeate flux and is given by the osmotic pressure model,

$$v_w = L_p(\Delta P - \Delta\pi) \quad (16)$$

ΔP is the transmembrane pressure difference and $\Delta\pi$ is the osmotic pressure difference across the membrane and L_p is the membrane permeability. The osmotic pressure difference across the membrane is given as,

$$\Delta\pi = \pi_m - \pi_p \quad (17)$$

where, π_m is the osmotic pressure at membrane surface and π_p is the same at the permeate stream. The osmotic pressure is generally expressed as a polynomial of concentration for macromolecules (Cheryan 1998),

$$\pi = a_1c + a_2c^2 + a_3c^3 \quad (18)$$

In context of osmotic pressure calculation, it is assumed that pH and electrolyte concentration of the solution is maintained constant throughout the experiments so that the charge on the macromolecule remains constant. However, in the simulation of the present work, dextran, an uncharged molecule is considered as the model solute.

The permeate concentration can be expressed in terms of the membrane surface concentration through the definition of real retention, which is constant for a particular membrane-solute system (Opong and Zydney 1991),

$$R_r = 1 - \frac{c_p}{c_m} \quad (19)$$

where, c_p is the solute concentration in permeate and c_m is that at membrane surface. Therefore, the osmotic pressure difference can be expressed in terms of the membrane surface concentration using Eqs. (17), (18) and (19),

$$\Delta\pi = a_1c_mR_r + a_2c_m^2[1 - (1 - R_r)^2] + a_3c_m^3[1 - (1 - R_r)^3] \quad (20)$$

The initial and boundary conditions of Eq. (14) are,

$$\text{for all } x \text{ and } y, \text{ at } t = 0, c = c_o \quad (21)$$

$$\text{for all } t \text{ and } y, \text{ at } x = 0, c = c_o \quad (22)$$

$$\text{for all } x \text{ and } t, \text{ at } y = h/2, \frac{\partial c}{\partial y} = 0 \quad (23)$$

$$\text{for all } x \text{ and } t, \text{ at } y = 0, D \frac{\partial c}{\partial y} + v_w c_m R_r = 0 \quad (24)$$

On solution of set of equations, Eqs. (14) to (24), the profile of permeate flux and permeate concentration are obtained as a function of time and channel length. The length averaged permeate flux and permeate concentration are expressed as,

$$v_{wa} = \frac{1}{L} \int_0^L v_w(x, t) dx \quad (25)$$

$$c_{pa} = \frac{1}{L} \int_0^L c_p(x, t) dx \quad (26)$$

The length averaged observed retention is defined as,

$$R_{oa} = 1 - \frac{c_{pa}}{c_0} \quad (27)$$

3. Results and discussions

3.1 Effect of pressure pulsation on velocity

It may be observed from Fig. 2, that the y-averaged velocity profile varies in a regular fashion about the mean velocity, *i.e.*, 0.3 m/s (considered herein). Imposition of this fluctuation of velocity will result in an oscillatory permeate flux without improving it over the long time. Therefore, the cross flow pulsation is required to be carried out as follows: the pulsation is continued as long as the velocity remains above the mean velocity *i.e.*, 0.3 m/s in this case. At the start of the pulsation, velocity increases and pulsation is stopped when it becomes u_0 *i.e.*, 0.3 m/s. Therefore, pulsation is imposed in the first half of the cycle as shown in Fig. 3. The velocity profile remains constant with the cross-sectional averaged velocity at u_o , in the next half of the cycle. Next pulsation starts at the end of the cycle. Pressure pulsation (cause) is manifested in velocity fluctuation (effect) and an explicit relationship is derived in this work between the two. However, the controller which will control this fluctuation will be designed to measure the resulting velocity change and act accordingly as per Fig. 3. Since an explicit relation between the pressure and velocity fluctuation is available, operation of controller can be done either by measuring the pressure or the resulting velocity.

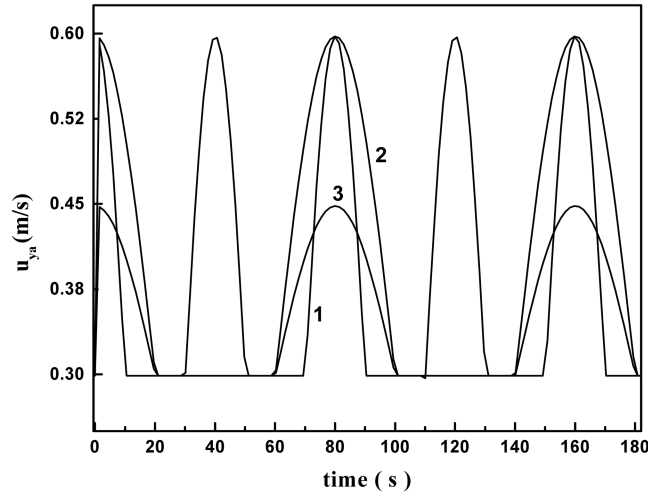


Fig. 3 Cross-sectional averaged velocity profile after imposition of the pulsation for half of the cycle, with k and ω at $\Delta P = 550$ kPa, $c_o = 10$ kg/m³ and $u_o = 0.3$ m/s (1) $k = 1.0$, $\omega = 0.157$ Hz; (2) $k = 1.0$, $\omega = 0.0785$ Hz; (3) $k = 0.5$, $\omega = 0.0785$ Hz

3.2 Solution to the convective diffusion equation ((Eq. (14)) for prediction of the permeate flux

The transient velocity profile, Eq. (10) is inserted in the transient mass balance equation, Eq. (14) and is solved using MATLAB. The duration of the flow rate pulsation is for the first half cycle as shown in Fig. 3. The simulation is carried out using dextran as the model solute. The physical properties of the solution, membrane permeability and the geometry of the flow channel are presented in the Table 1.

Fig. 4 shows the variation of the length averaged membrane surface concentration with time for different values of amplitude and frequency of pulsation. The predictions are compared with the transient solution without pulsation (curve 4). It may be observed from the figure that the membrane surface concentration is mainly influenced by the amplitude of pulsation. The profile of the membrane surface concentration qualitatively follows the imposed velocity pulsation as shown in Fig. 3. Higher the amplitude, lower is the membrane surface concentration (curves 1 and 2 versus 3) due to higher shear induced effects. The corresponding length averaged permeate flux profiles are

Table 1 Channel geometry and the physical properties of the solute, solution and membrane

Solute diffusivity: 4×10^{-11} m ² /s
Membrane permeability: 2.46×10^{-11} m/Pa.s
Osmotic pressure coefficients: $a_1 = 37.5$
$a_2 = 0.754$
$a_3 = 0.00764$
Length of channel: 1.0 m
Width of the channel: 0.04 m
Height of the channel :0.001 m

shown in Fig. 5. Here also, the permeate flux profiles follow the trend of the imposed cross flow velocity fluctuations. The upper half cycle pulsation increases the permeate flux and it is more for larger amplitude.

The length averaged permeate flux profiles for various values of R_r are shown in Fig. 6. For each

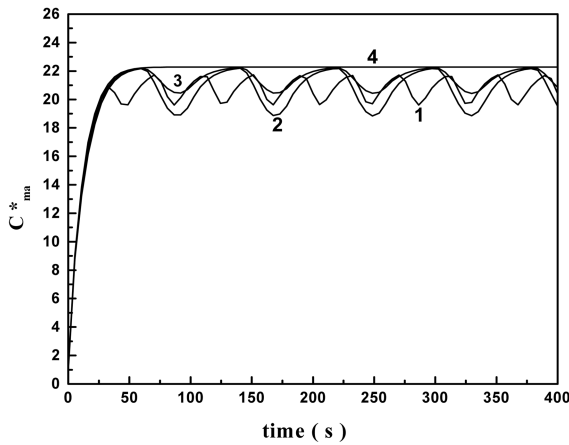


Fig. 4 Variation of length averaged dimensionless membrane surface concentration with time for different values of k and ω at $\Delta P = 550$ kPa, $c_0 = 10$ kg/m³, $u_0 = 0.3$ m/s and $R_r = 1.0$ (1) $k = 1.0$, $\omega = 0.157$ Hz; (2) $k = 1.0$, $\omega = 0.0785$ Hz; (3) $k = 0.5$, $\omega = 0.0785$ Hz; (4) without pulsation

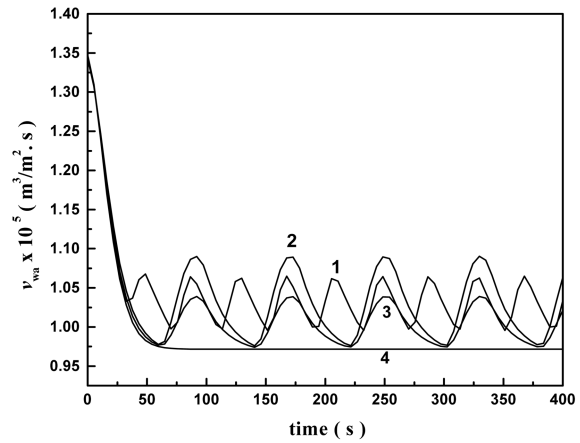


Fig. 5 Variation of length averaged permeate flux with time for different values of k and ω at $\Delta P = 550$ kPa, $c_0 = 10$ kg/m³, $u_0 = 0.3$ m/s and $R_r = 1.0$ (1) $k = 1.0$, $\omega = 0.157$ Hz; (2) $k = 1.0$, $\omega = 0.0785$ Hz; (3) $k = 0.5$, $\omega = 0.0785$ Hz; (4) without pulsation

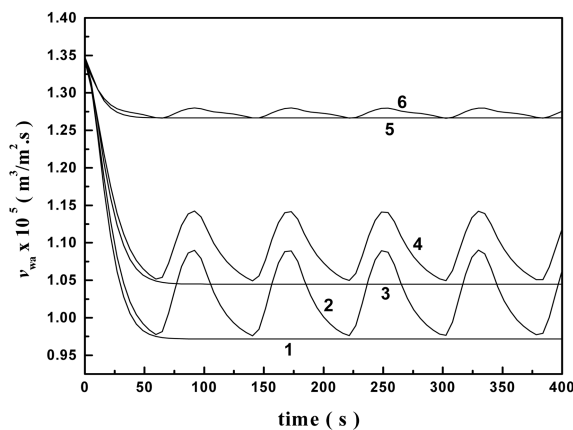


Fig. 6 Variation of length average permeate flux with time for different values of R_r at $\Delta P = 550$ kPa, $c_0 = 10$ kg/m³, $u_0 = 0.3$ m/s and $k = 1.0$, $\omega = 0.0785$ Hz (1) and (2) $R_r = 1.0$; (3) and (4) $R_r = 0.99$; (5) and (6) $R_r = 0.95$. (1), (3) and (5) are for without pulsation

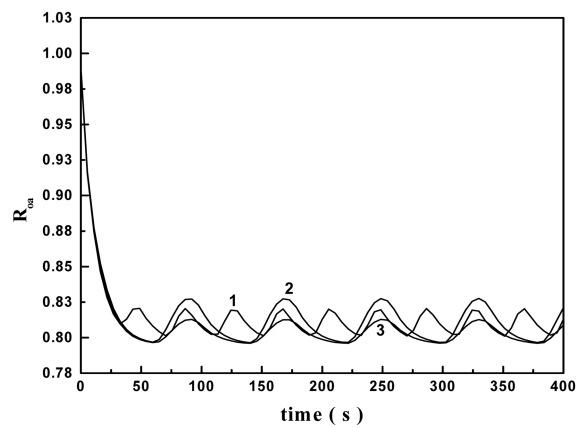


Fig. 7 Variation of length average observed retention with k and ω at $\Delta P = 550$ kPa, $c_0 = 10$ kg/m³, $u_0 = 0.3$ m/s and $R_r = 0.99$ (1) $k = 1.0$, $\omega = 0.157$ Hz; (2) $k = 1.0$, $\omega = 0.0785$ Hz; (3) $k = 0.5$, $\omega = 0.0785$ Hz

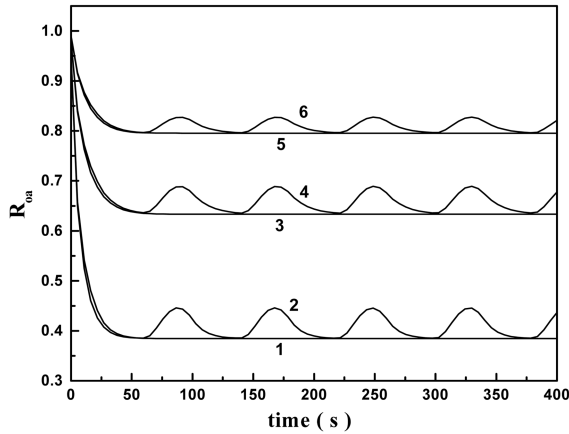


Fig. 8 Variation of length averaged observed retention with R_r at $\Delta P = 550$ kPa, $c_0 = 10$ kg/m³, $u_o = 0.3$ m/s and $k = 1.0$, $\omega = 0.0785$ Hz (1) and (2) $R_r = 0.95$; (3) and (4) $R_r = 0.98$; (5) and (6) $R_r = 0.99$. 1, 3 and 5 are for without pulsation.

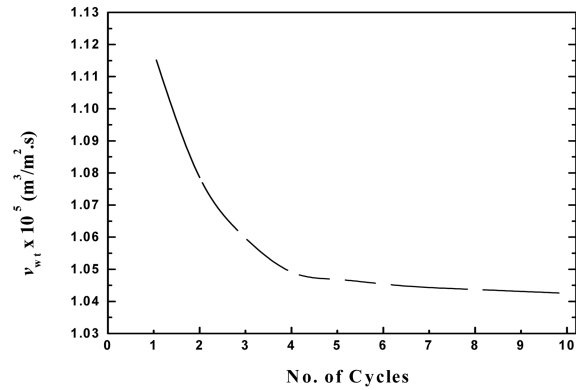


Fig. 9 Variation of time averaged, length averaged permeate flux with number of cycles at $\Delta P = 550$ kPa, $c_0 = 10$ kg/m³, $u_o = 0.3$ m/s, $R_r = 1.0$, $k = 1.0$, $\omega = 0.157$ Hz

R_r , the corresponding case of without pulsation is also presented. As expected, the flux increases with lowering of R_r . The effect of pulsation merits further discussion. It may be observed from the figure that as the membrane becomes more porous (less real retention), the effect of pulsation is dampened. For example, for $R_r = 0.95$ there is insignificant improvement of the permeate flux, due to pulsation. As the membrane becomes more porous, the solute build up over it will be less and hence, the membrane surface concentration is less as well. Therefore, the scouring effect of the pulsation in the cross flow velocity in terms of reduction in c_m and increase in the permeate flux becomes less prominent. Therefore, the effect of the cross flow pulsation is minimized as the value of R_r becomes smaller.

The variation of the length averaged observed retention (R_{0a}) is shown in Fig. 7 for $R_r = 0.99$ at various pulse amplitude and frequency. It may be observed that the long term time averaged observed retention increases with pulsation and it is more for higher amplitude of pulses. The effects of pulsation on the length averaged observed retention with different R_r values are shown in Fig. 8. It is observed that R_{0a} increases with pulsation but for more open membranes (lower R_r), the effect becomes more as discussed earlier.

Selection of the number of cycles for long term time averaging

In order to establish the suitable operating amplitude and frequency of the flow rate pulsation, one must compute the long term time averaged permeate flux. For this purpose, the length averaged permeate flux is time averaged over a number of time cycles. The results are presented in Fig. 9. As observed from the figure, the time-averaged, length averaged permeate flux is independent of the number of cycles after about 4 cycles. Therefore, all time averaging of the permeate flux is computed over 4 cycles of oscillation.

3.2.1 Selection of the operating parameters of the pulsation

The variation of length averaged, long term time averaged (over four cycles) permeate flux with frequency of pulsation is shown in Fig. 10 for various amplitudes. It is observed from the figure

that there is insignificant flux enhancement with the frequency of the pulsation. It is observed that the permeate flux increase from 1.013×10^{-6} m/s to 1.058×10^{-6} m/s as k increase from 0.5 to 2.

Limit of the amplitude of pulsation

As discussed earlier, the amplitude (k) plays the most important part in flux improvements. The amplitude is associated with the fluctuations in the pressure drop. It is clear that the fluctuations in pressure drop leads to the corresponding variation in velocity u . Since, the analysis in the present work is valid strictly in laminar flow regime ($Re < 2200$), maximum amplitude of fluctuation corresponding to the steady state velocity (u_0) is estimated by calculating u from Eq. (10) so that the Reynolds number is less than 2200. Table 2 shows the maximum value of the amplitude that can be selected for a particular cross-sectional averaged cross flow velocity (u_0) (under steady state around which the pulsation is resulted). Using this value of k_{max} , the length and long term time averaged permeate flux values are computed with and without pulsation and are presented in Fig. 11. The percentage increases in flux for various u_0 values are shown in Table 3. It is clear from Table 3 and Fig. 12 that for lower cross flow velocities, the flow rate pulsation is more effective and one can get

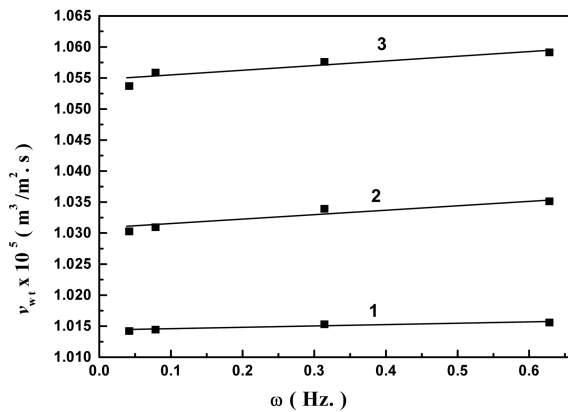


Fig. 10 Variation of length averaged, time averaged permeate flux with ω at $\Delta P = 550$ kPa, $c_0 = 10$ kg/m³, $u_0 = 0.3$ m/s and $R_r = 1.0$. (1) $k = 0.5$; (2) $k = 1.0$; (3) $k = 2.0$

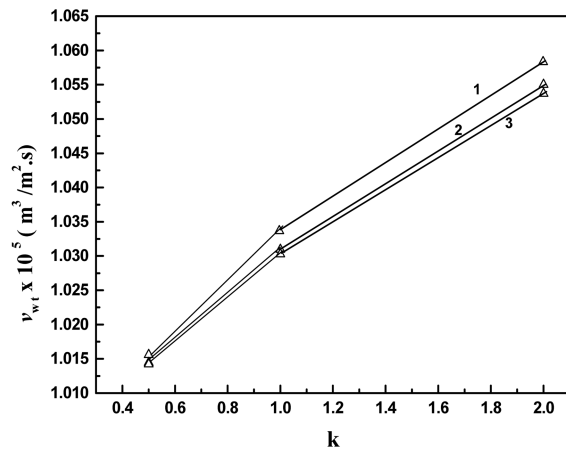


Fig. 11 Variation of length averaged, time averaged permeate flux with k at $\Delta P = 550$ kPa, $c_0 = 10$ kg/m³, $u_0 = 0.3$ m/s and $R_r = 1.0$ (1) $\omega = 0.628$ Hz; (2) $\omega = 0.0785$ Hz; (3) $\omega = 0.0418$ Hz

Table 2 Maximum amplitude that can be selected maintaining the laminar flow regime

u_0 (m/s)	k_{max}
0.1	10
0.2	4.6
0.3	2.75
0.4	1.8
0.6	0.85
0.8	0.39
1.1	0

Table 3 Length averaged, time averaged permeate flux with and without pulsation for different values of u_o and the percentage increase in permeate flux

u_o (m/s)	$v_{wt} \times 10^5$ (m/s) with Pulsation	$v_{wt} \times 10^5$ (m/s) without pulsation	% increase in flux
1.1	1.21	1.21	0
0.8	1.18	1.16	1.27
0.6	1.15	1.12	3.03
0.3	1.09	0.99	9.76
0.2	1.06	0.91	15.73
0.1	1.01	0.78	29.02

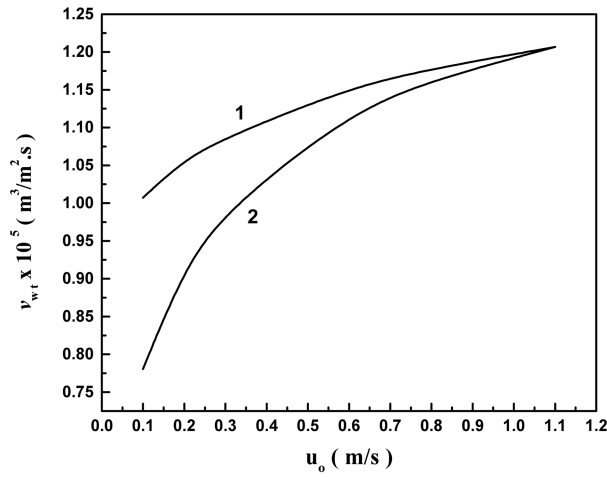


Fig. 12 Comparison of length average time average permeate flux with and without pulsation, at different cross sectional average velocity (1) with pulsation (using $k = k_{max}$ as in Table 1); (2) without pulsation

a flux enhancement upto 29%, whereas, this will not be effective for higher cross flow velocity.

4. Conclusions

In the present work, an attempt has been made to quantify the extent of flux enhancement possible in an osmotic pressure controlled cross flow ultrafiltration system under the laminar flow regime, using transmembrane pressure pulsation. In the model developed herein, the transient velocity profile is solved analytically and the analytic results are verified numerically. The coupled hydrodynamic and mass transfer problem is solved to obtain the membrane surface concentration and the permeate flux as functions of the operating conditions, namely, the real retention, amplitudes and frequencies of pulsation, etc. It is observed that the pulse amplitude plays the most important role in the flux improvement, whereas an insignificant flux enhancement occurs with the frequency of the pulsation. For lower cross flow velocities, the pulsation is most effective and flux enhancement up to 29% can be achieved for dextran solution.

References

- Ahmad, A.L., Lau, K.K. and Abu Bakar, M.Z. (2005), "Impact of different spacer filament geometries on concentration polarization control in narrow membrane channel", *J. Membrane Sci.*, **208**, 138-152.
- Bertram, C.D., Hoogland, M.R., Li, H., Odell, R.A. and Fane, A.G. (1993), "Flux enhancement in crossflow microfiltration using a collapsible tube pulsation generator", *J. Membrane Sci.*, **84**, 279-292.
- Bird, R.B., Stewart, W.E. and Lightfoot, E.N. (2002), *Transport Phenomena*, John Wiley and Sons, Inc., Singapore.
- Bouchard, C.R., Carreau, P.J., Matsuuara, T. and Sourirajan, S. (1994), "Modeling of ultrafiltration: predictions of concentration polarization effects", *J. Membrane Sci.*, **97**, 215-229.
- Cheryan, M. (1998), *Ultrafiltration and microfiltration handbook*, Technomic Publishing Co., Lancaster.
- Curcio, S., Calabrd, V. and Iorio, G. (2002), "Monitoring and control of TMP and feed flow rate pulsatile operations during ultrafiltration in a membrane module", *Desalination*, **146**, 217-222.
- Das, C., DasGupta, S. and De, S. (2007), "Treatment of soaking effluent from tannery using membrane separation processes", *Desalination*, **216**, 160-173.
- Das, C., De, S. and DasGupta, S. (2008), "Treatment of liming effluent from tannery using membrane separation processes", *Sep. Sci. Technol.*, **42**, 517-539.
- Doraiswamy, R., Amundson, N.R. (1985), *Linear operator method in chemical engineering with applications to transport and chemical reaction systems*, Prentice Hall, New Jersey, USA.
- Gupta, B.B., Blanpain, P. and Jaffrin, M.Y. (1992), "Permeate flux enhancement by pressure and flow pulsation in microfiltration with mineral membranes", *J. Membrane Sci.*, **70**, 256-266.
- Hadzismajlovic, D.E. and Bertram, C.D. (1998a), "Flux enhancement in laminar cross flow microfiltration using a collapsible tube pulsation generator", *J. Membrane Sci.*, **142**, 173-189.
- Hadzismajlovic, D.E. and Bertram, C.D. (1998b), "Flux enhancement in turbulent cross flow microfiltration using a collapsible tube pulsation generator", *J. Membrane Sci.*, **163**, 123-134.
- Ilias, S. and Govind R. (1997), "Potential applications of pulsed flow for minimizing concentration polarization in ultrafiltration", *Sep. Sci. Technol.*, **25**, 1307-1324.
- Jaffrin, M.Y. (1989), "Innovative process for membrane plasma separation", *J. Membrane Sci.*, **44**, 115-129.
- Jaffrin, M.Y., Gupta, B.B. and Paultier, P. (1994), "Energy saving pulsatile mode cross flow Filtration", *J. Membrane Sci.*, **86**, 281-290.
- Krstic, D.M., Tekic, M.N., Caric, M.D. and Milanovic, S.D. (2002), "Effect of turbulent promoter on crossflow microfiltration of skim milk", *J. Membrane Sci.*, **208**, 303-314.
- Li, H. and Bertram, C.D. and Wiley, D.E. (1998), "Mechanisms by which pulsatile flow affects cross flow microfiltration", *AIChE J.*, **44**, 1950-1961.
- Najarian, S. and Bellhouse, B.J. (1996), "Effect of liquid pulsation on protein fractionation using ultrafiltration processes", *J. Membrane Sci.*, **114**, 245-253.
- Opong, W.S. and Zydney, A.L. (1991), "Diffusive and convective protein transport through asymmetric membranes", *AIChE J.*, **37**, 1497-1512.
- Pal, S., Ghatak, S., De, S. and DasGupta, S. (2008a), "Evaluation of surface roughness of a plasma treated polymeric membrane by wavelet analysis and quantification of its enhanced performance", *Appl. Surf. Sci.*, **255**, 2504-2511.
- Pal, S., Ghatak, S.K., DasGupta, S. and De, S. (2008b), "Characterization of CO₂ plasma treated polymeric membranes and quantification of flux enhancement", *J. Membrane Sci.*, **323**(1-10), 2008.
- Prádanos, P., Hernández, A., Calvo, J.I. and Tejerina, F. (1996), "Mechanisms of protein fouling in cross-flow UF through an asymmetric inorganic membrane", *J. Membrane Sci.*, **114**, 115-126.
- Rodgers, V.G.J. and Sparks, R.E. (1991), "Reduction of membrane fouling in the ultrafiltration of binary protein mixtures", *AIChE J.*, **37**, 1517-1528.
- Rodgers, V.G.J. and Sparks, R.E. (1992), "Effect of transmembrane pressure pulsing on concentration polarization", *J. Membrane Sci.*, **68**, 149-168.
- Sarkar, B., DasGupta, S. and De, S. (2008a), "Cross-flow electro-ultrafiltration of mosambi (Citrus Sinensis (L.) Osbeck) juice", *J. Food Eng.*, **89**, 241-245.
- Sarkar, B., DasGupta, S. and De, S. (2008b) "Prediction of permeate flux during osmotic pressure controlled

- electric field enhanced cross flow ultrafiltration”, *J. Colloid Interf. Sci.*, **319**, 236-246.
- Sarkar, B., DasGupta, S. and De, S. (2008c) “Effect of electric field during gel-layer controlled ultrafiltration of synthetic and fruit juice”, *J. Membrane Sci.*, **307** (2), 268-276.
- Spiazi, E., Lenoir, J. and Grangeon, A. (1993), “A new generator of unsteady state flow regime in tubular membranes as anti-fouling technique: A hydrodynamic approach”, *J. Membrane Sci.*, **80**, 49-57.
- Wakeman, R.J. and Williams, C.J. (2002), “Additional techniques to improve microfiltration”, *Sep. Purif. Technol.*, **26**, 3-28.
- Wang, W., Bertram, C.D. and Wiley, D.E. (2007), “Effects of collapsible-tube-induced pulsation vigour on membrane filtration performance”, *J. Membrane Sci.*, **288**, 298-306.
- Wang, Y., Howell, J.A., Field, R.W. and Wu, D. (1994), “Simulation of cross flow filtration for baffled tubular channels and pulsatile flow”, *J. Membrane Sci.*, **95**, 243-258.
- Winzeler, H. B. and Belfort, G. (1993), “Enhanced performance for pressure driven membrane processes: The argument for fluid instabilities”, *J. Membrane Sci.*, **80**, 35-47.

CC

Nomenclature

$A_{1,2}$	constants in Eq. (A17)
$a_{1,2,3}$	osmotic pressure coefficients in Eq. (18)
a_n	time varying part of Green’s function
c	solute concentration [kg/m ³]
c_o	feed solute concentration at the channel inlet [kg/m ³]
c_m	membrane surface concentration [kg/m ³]
c_p	solute concentration in permeate [kg/m ³]
c_{pa}	length averaged solute concentration in permeate [kg/m ³]
D	solute diffusivity [m ² /s]
g	Green’s function
g^*	Adjoint Green’s function
h	channel height [m]
k	amplitude of pulsation [Hz]
L	channel length [m]
L_1	operator
L^*_1	operator
L_p	membrane Permeability [m/s Pa]
P	Pressure [Pa]
$P_{permeate}$	Pressure in the permeate side [Pa]
R_r	real retention
t	time [s]
t^*_0	time coordinate of unit impulse in Green’s function
t^*_1	time coordinate of unit impulse in adjacent Green’s function
u	axial velocity [m/s]
u^*	dimensionless velocity
u_{ya}^*	dimensionless cross-sectional pulsatile average velocity [m/s]
u_o	cross-sectional steady state average velocity [m/s]
v	velocity in y-direction [m/s]
v_w	permeate flux [m ³ /m ² .s]
v_{wa}	length averaged permeate flux [m ³ /m ² .s]
v_{wt}	length averaged time averaged permeate flux [m ³ /m ² .s]
x	axial dimension [m]
y	transverse dimension [m]

y_0^*	space coordinate of unit impulse in Green's function
y_1^*	time coordinate of unit impulse in adjacent Green's function

Greek symbols

α	dimensionless pressure gradient
β	dimensionless frequency
ΔP	transmembrane pressure difference at any x location [Pa]
$(\Delta P)_i$	transmembrane pressure difference at the inlet of the channel [Pa]
Φ_n	n-th eigenfunction
λ_n	n-th eigenvalue
π	osmotic pressure [Pa]
π_m	osmotic pressure at the membrane surface [Pa]
π_p	osmotic pressure at the permeate side [Pa]
$\Delta\pi$	osmotic pressure difference across the membrane [Pa]
ν	kinematic viscosity [m^2/s]
μ	viscosity [Pa s]
ω	frequency of pulsation [Hz]
ρ	density [kg/m^3]

Appendix

Transient velocity profile using Green's function (Doriaswamy and Amundson 1985):

The governing equation of the transient velocity is given by Eq. (6) with initial and boundary conditions expressed in Eq. (7) to (9),

Eq. (6) can be expressed as

$$L_1 u^* = \alpha[1 + k \cos(\beta t^*)] \quad (\text{A1})$$

where, the operator $L_1 = \frac{\partial}{\partial t} - \frac{\partial^2}{\partial y^{*2}}$. The right hand side of Eq. (A1) can be treated as a source term.

Since the governing equation, Eq. (A1) is a linear, non-homogeneous type, a solution using green's function is sought.

The causal Green's function is constructed as,

$$\frac{\partial g(y^*, t^*/y_0^*, t_0^*)}{\partial t^*} - \frac{\partial^2 g(y^*, t^*/y_0^*, t_0^*)}{\partial y^{*2}} = \delta(y^* - y_0^*) \delta(t^* - t_0^*) \quad (\text{A2})$$

where, g is the causal Green's function, δ is the dirac delta function and y_0^*, t_0^* are the location of impulse in dirac delta function. The initial and boundary conditions of Eq. (A2) are

$$\text{for all } y^*, \text{ at } t^* = 0, g^* = 0 \quad (\text{A3})$$

$$\text{for all } t^*, \text{ at } y^* = 0, g^* = 0 \quad (\text{A4})$$

$$y^* = 0, g^* = 0 \quad (\text{A5})$$

Using partial eigenfunction expansion, Green's function can be expressed as,

$$g(y^*, t^*/y_0^*, t_0^*) = \sum_{n=1}^{\infty} a_n(t^*) \Phi_n(y^*) \quad (\text{A6})$$

where, Φ_n is n th eigenfunction (spatial part) and a_n is the time varying part. The spatial part of Eq. (A6) must satisfy the following eigenvalue problem.

$$\frac{d^2 \Phi_n}{dy^{*2}} + \lambda_n^2 \Phi_n = 0 \quad (\text{A7})$$

$$\text{Subject to, } \Phi_n = 0 \text{ at } y^* = 0 \quad (\text{A8})$$

$$\text{and } \Phi_n = 0 \text{ at } y^* = 1 \quad (\text{A9})$$

Solution of Eq. (A7) with the boundary conditions are,

$$\Phi_n(y^*) = C_1 \text{Sin}(\lambda_n y^*) \quad (\text{A10})$$

where $\lambda_n = n\pi$, $n = 1, 2, \dots, \infty$ are the eigenvalues.

Forcing $\Phi_n(y^*)$ to be orthonormal *i.e.*, $\|\Phi_n\|^2 = 1$, the value of C_1 is obtained as $C_1 = \sqrt{2}$. Therefore, the complete solution of Eq. (A7) is,

$$\Phi_n(y^*) = \sqrt{2} \text{Sin}(\lambda_n y^*) \tag{A11}$$

Using orthogonal properties of sin functions, $a_n(t^*)$ becomes ((from Eq. (A6)),

$$a_n(t^*) = \frac{\langle g, \Phi_n \rangle}{\langle \Phi_n, \Phi_n \rangle} \tag{A12}$$

where, $\langle f_1, f_2 \rangle$ represents the inner product of functions f_1 and f_2 .

Since, Φ_n are orthonormal as well, the expression of a_n becomes,

$$a_n(t^*) = \langle g, \Phi_n \rangle \tag{A13}$$

Taking inner product of Eq. (A2) with Φ_n , the following expression is obtained,

$$\frac{d\langle g, \Phi_n \rangle}{dt^*} - \int_0^1 \frac{\partial^2 g}{\partial y^{*2}} dy^* = \int_0^1 \delta(y^* - y_0^*) \delta(t^* - t_0^*) \Phi_n dy^* \tag{A14}$$

Using Eq. (A7) and its boundary conditions Eqs. (A8) and (A9), the governing equation of a_n is obtained after simplification,

$$\frac{da_n}{dt^*} + \lambda_n^2 a_n = \delta(t^* - t_0^*) \Phi_n(y_0^*) \tag{A15}$$

In order to obtain the solution of a_n , the following equation is considered,

$$\frac{da_n}{dt^*} + \lambda_n^2 a_n = 0 \tag{A16}$$

The solution of Eq. (A16) becomes,

$$\begin{aligned} a_n(t^*) &= A_1 \exp(-\lambda_n^2 t^*) \text{ for } t^* < t_0^* \\ &= A_2 \exp(-\lambda_n^2 t^*) \text{ for } t^* > t_0^* \end{aligned} \tag{A17}$$

Since as $t^* = 0$, $g = 0$ and hence $a_n = 0$ and therefore $A_1 = 0$

Integrating Eq. (A15) between t_0^{*-} and t_0^{*+} ,

$$a_n(t_0^{*+}) = \Phi_n(y_0^*) \tag{A18}$$

Combining Eqs. (A18) and (A17), the value of A_2 is obtained,

$$A_2 = \Phi_n(y_0^*) \exp(-\lambda_n^2 t_0^*) \tag{A19}$$

Thus, the solution of a_n becomes,

$$\begin{aligned} a_n(t^*) &= 0 && \text{for } t^* < t_0^* \\ &= \Phi_n(y_0^*) \exp[-\lambda_n^2(t^* - t_0^*)] && \text{for } t^* > t_0^* \end{aligned} \quad (\text{A20})$$

Thus the Green's function becomes,

$$\begin{aligned} g(y^*, t^*/y_0^*, t_0^*) &= 0 && \text{for } t^* < t_0^* \\ &= \sum_{n=1}^{\infty} \Phi_n(y^*) \Phi_n(y_0^*) \exp[-\lambda_n^2(t^* - t_0^*)] && \text{for } t^* > t_0^* \end{aligned} \quad (\text{A21})$$

Having obtained Green's function, the adjoint Green's function is constructed. The adjoint operator corresponding to L_1 is (Doriaswamy and Amundson 1985),

$$L_1^* = \frac{\partial}{\partial t^*} - \frac{\partial^2}{\partial y^{*2}}$$

Therefore, the governing equation of adjoint Green's function becomes,

$$-\frac{\partial g^*(y^*, t^*/y_1^*, t_1^*)}{\partial t^*} - \frac{\partial^2 g^*(y^*, t^*/y_1^*, t_1^*)}{\partial y^{*2}} = \delta(y^* - y_1^*) \delta(t^* - t_1^*) \quad (\text{A22})$$

where, g^* is the adjoint Green's function and y_1^*, t_1^* are the corresponding variables. Now, the inner product of Eq. (A2) with g^* and that Eq. (A22) with g are taken and subtracted. By forcing bilinear concomittant to be zero, the relationship between g and g^* and initial and boundary conditions of g^* are obtained,

$$g^*(y_0^*, t_0^*/y_1^*, t_1^*) = g(y_1^*, t_1^*/y_0^*, t_0^*) \quad (\text{A23})$$

$$\text{for } t^* > t_1^*, g^* = 0 \quad (\text{A24})$$

$$\text{for } y^* = 0, g^* = 0 \quad (\text{A25})$$

$$\text{for } y^* = 1, g^* = 0 \quad (\text{A26})$$

Taking inner product of Eq. (7) with g^* and that of Eq. (A22) with u^* and after subtraction, the following equation is resulted,

$$\begin{aligned} &\int_0^{t_1^*} \int_0^1 \frac{\partial u^*}{\partial t^*} g^* dy^* dt^* - \int_0^{t_1^*} \int_0^1 \frac{\partial^2 u^*}{\partial y^{*2}} g^* dy^* dt^* + \int_0^{t_1^*} \int_0^1 \frac{\partial g^*}{\partial t^*} u^* dy^* dt^* + \int_0^{t_1^*} \int_0^1 \frac{\partial^2 g^*}{\partial y^{*2}} u^* dy^* dt^* \\ &= a \int_0^{t_1^*} \int_0^1 (1 + k \cos \beta t^*) g^* dy^* dt^* - u^*(y_1^*, t_1^*) \end{aligned} \quad (\text{A27})$$

Using the relationship between g and g^* (Eq. (A23)) and the boundary conditions of u^* (Eqs. (9) and (10)) and g^* (Eqs. (A25), (A26)), and simplification, Eq. (A27) becomes,

$$\begin{aligned} u^*(y_1^*, t_1^*) &= \int_0^1 u^*(t_0^*=0) g^*(y_0^*, 0/y_1^*, t_1^*) dy_0^* dt_0^* + a \int_0^1 \int_0^1 (1+k \cos \beta t_0^*) g^* dy_0^* dt_0^* \\ &= I_1 + I_2 \end{aligned} \quad (\text{A28})$$

The integral I_1 is,

$$\begin{aligned} I_1 &= \int_0^1 6(y_0^* - y_0^{*2}) \sum_{n=1}^{\infty} \Phi_n(y_1^*) \Phi_n(y_0^*) \exp(-\lambda_n^2 t_1^*) dy_0^* \\ &= 24 \sum_{n=1}^{\infty} \frac{(1-\cos(n\pi))}{n^3 \pi^3} \sin(n\pi y_1^*) e^{-n^2 \pi^2 t_1^*} \end{aligned} \quad (\text{A29})$$

Substituting expression for g^* , the integral I_2 is evaluated as,

$$I_2 = 2a \sum_{n=1}^{\infty} \frac{(1-\cos n\pi)}{n\pi} \sin(n\pi y_1^*) \left[\frac{1-e^{-n^2 \pi^2 t_1^*}}{n^2 \pi^2} + \frac{k}{n^4 \pi^4 + \beta^2} (n^2 \pi^2 \cos \beta t_1^* + \beta \sin \beta t_1^* - n^2 \pi^2 e^{-n^2 \pi^2 t_1^*}) \right] \quad (\text{A30})$$

Changing the coordinates y_1^*, t_1^* to y^*, t^* the velocity profile is,

$$\begin{aligned} u^*(y^*, t^*) &= 24 \sum_{n=1}^{\infty} \frac{(1-\cos(n\pi))}{n^3 \pi^3} \sin(n\pi y^*) e^{-n^2 \pi^2 t^*} \\ &+ 2a \sum_{n=1}^{\infty} \frac{(1-\cos n\pi)}{n\pi} \sin(n\pi y^*) \left[\frac{1-e^{-n^2 \pi^2 t^*}}{n^2 \pi^2} + \frac{k}{n^4 \pi^4 + \beta^2} (n^2 \pi^2 \cos \beta t^* + \beta \sin \beta t^* - n^2 \pi^2 e^{-n^2 \pi^2 t^*}) \right] \end{aligned} \quad (\text{A31})$$